Enhancing and redirecting carbon nanotube photoluminescence by an optical antenna

Miriam Böhmler,[1] Nicolai Hartmann,[1] Carsten Georgi,[1] Frank Hennrich,[2] Alexander A. Green,[3] Mark C. Hersam,[3] and Achim Hartschuh[1,*]

[1]*Department Chemie and CeNS, Ludwig-Maximilians-Universität München, 81377 München, Germany*
[2]*Forschungszentrum Karlsruhe GmbH, Institut für Nanotechnologie, 76021 Karlsruhe, Germany*
[3]*Department of Materials Science and Engineering, Department of Chemistry, Northwestern University, Evanston, Illinois 60208-3108, USA*
**achim.hartschuh@cup.uni-muenchen.de*

Abstract: We observe the angular radiation pattern of single carbon nanotubes' photoluminescence in the back focal plane of a microscope objective and show that the emitting nanotube can be described by a single in-plane point dipole. The near-field interaction between a nanotube and an optical antenna modifies the radiation pattern that is now dominated by the antenna characteristics. We quantify the antenna induced excitation and radiation enhancement and show that the radiative rate enhancement is connected to a directional redistribution of the emission.

OCIS codes: (160.6000) Semiconductor materials; (180.4243) Near-field microscopy; (260.3800) Luminescence; (260.3910) Metal optics.

References and links

1. A. Jorio, M. S. Dresselhaus, and G. Dresselhaus, eds., *Carbon Nanotubes*, vol. 111 of Topics in Applied Physics (Springer, Berlin / Heidelberg, 2008).
2. J. Lefebvre, S. Maruyama, and P. Finnie, *"Photoluminescence: Science and Applications"* in *Carbon Nanotube*s, vol. 111 of Topics in Applied Physics, A. Jorio, M. S. Dresselhaus, and G. Dresselhaus, eds. (Springer, Berlin / Heidelberg, 2008).
3. P. Avouris, M. Freitag, and V. Perebeinos, "Carbon-nanotube photonics and optoelectronics," Nat. Photonics **2**(6), 341–350 (2008).
4. F. Xia, M. Steiner, Y. M. Lin, and P. Avouris, "A microcavity-controlled, current-driven, on-chip nanotube emitter at infrared wavelengths," Nat. Nanotechnol. **3**(10), 609–613 (2008).
5. J. A. Schuller, E. S. Barnard, W. Cai, Y. C. Jun, J. S. White, and M. L. Brongersma, "Plasmonics for extreme light concentration and manipulation," Nat. Mater. **9**(3), 193–204 (2010).
6. P. Bharadwaj, B. Deutsch, and L. Novotny, "Optical Antennas," Adv. Opt. Photon. **1**(3), 438–483 (2009).
7. J. N. Farahani, D. W. Pohl, H.-J. Eisler, and B. Hecht, "Single quantum dot coupled to a scanning optical antenna: a tunable superemitter," Phys. Rev. Lett. **95**(1), 017402 (2005).
8. J. N. Anker, W. P. Hall, O. Lyandres, N. C. Shah, J. Zhao, and R. P. Van Duyne, "Biosensing with plasmonic nanosensors," Nat. Mater. **7**(6), 442–453 (2008).
9. E. Fort, and S. Grésillon, "Surface enhanced fluorescence," J. Phys. D **41**(1), 013001 (2008).
10. A. Hartschuh, "Tip-enhanced near-field optical microscopy," Angew. Chem. Int. Ed. Engl. **47**(43), 8178–8191 (2008).
11. V. Deckert, "Tip-Enhanced Raman Spectroscopy," J. Raman Spectrosc. **40**(10), 1336–1337 (2009).
12. P. Bharadwaj, and L. Novotny, "Spectral dependence of single molecule fluorescence enhancement," Opt. Express **15**(21), 14266–14274 (2007).
13. L. G. Cançado, A. Hartschuh, and L. Novotny, "Tip-enhanced Raman spectroscopy of carbon nanotubes," J. Raman Spectrosc. **40**(10), 1420–1426 (2009).
14. R. Ruppin, "Decay of an excited molecule near a small metal sphere," J. Chem. Phys. **76**(4), 1681–1684 (1982).
15. H. Gersen, M. F. García-Parajó, L. Novotny, J. A. Veerman, L. Kuipers, and N. F. van Hulst, "Influencing the angular emission of a single molecule," Phys. Rev. Lett. **85**(25), 5312–5315 (2000).
16. S. Kühn, G. Mori, M. Agio, and V. Sandoghdar, "Modification of single molecule fluorescence close to a nanostructure: radiation pattern, spontaneous emission and quenching," Mol. Phys. **106**(7), 893–908 (2008).
17. T. H. Taminiau, F. D. Stefani, and N. F. van Hulst, "Single emitters coupled to plasmonic nano-antennas: angular emission and collection efficiency," N. J. Phys. **10**(10), 105005 (2008).
18. T. H. Taminiau, F. D. Stefani, F. B. Segerink, and N. F. van Hulst, "Optical antennas direct single-molecule emission," Nat. Photonics **2**(4), 234–237 (2008).
19. C. Huang, A. Bouhelier, G. Colas des Francs, A. Bruyant, A. Guenot, E. Finot, J.-C. Weeber, and A. Dereux, "Gain, detuning, and radiation patterns of nanoparticle optical antennas," Phys. Rev. B **78**(15), 155407 (2008).

#128057 - $15.00 USD Received 5 May 2010; revised 24 Jun 2010; accepted 6 Jul 2010; published 21 Jul 2010

20. P. Anger, P. Bharadwaj, and L. Novotny, "Enhancement and quenching of single-molecule fluorescence," Phys. Rev. Lett. **96**(11), 113002 (2006).
21. H. Qian, P. T. Araujo, C. Georgi, T. Gokus, N. Hartmann, A. A. Green, A. Jorio, M. C. Hersam, L. Novotny, and A. Hartschuh, "Visualizing the local optical response of semiconducting carbon nanotubes to DNA-wrapping," Nano Lett. **8**(9), 2706–2711 (2008).
22. M. S. Arnold, A. A. Green, J. F. Hulvat, S. I. Stupp, and M. C. Hersam, "Sorting carbon nanotubes by electronic structure using density differentiation," Nat. Nanotechnol. **1**(1), 60–65 (2006).
23. N. Stürzl, F. Hennrich, S. Lebedkin, and M. M. Kappes, "Near Monochiral Single-Walled Carbon Nanotube Dispersions in Organic Solvents," J. Phys. Chem. C **113**(33), 14628–14632 (2009).
24. M. A. Lieb, J. M. Zavislan, and L. Novotny, "Single-molecule orientations determined by direct emission pattern imaging," J. Opt. Soc. Am. B **21**(6), 1210–1215 (2004).
25. C. Georgi, N. Hartmann, T. Gokus, A. A. Green, M. C. Hersam, and A. Hartschuh, "Photoinduced luminescence blinking and bleaching in individual single-walled carbon nanotubes," ChemPhysChem **9**(10), 1460–1464 (2008).
26. L. Cognet, D. A. Tsyboulski, J. D. R. Rocha, C. D. Doyle, J. M. Tour, and R. B. Weisman, "Stepwise quenching of exciton fluorescence in carbon nanotubes by single-molecule reactions," Science **316**(5830), 1465–1468 (2007).
27. G. Y. Slepyan, M. V. Shuba, S. A. Maksimenko, and A. Lakhtakia, "Theory of optical scattering by achiral carbon nanotubes and their potential as optical nanoantennas," Phys. Rev. B **73**(19), 195416 (2006).
28. A. Hagen, M. Steiner, M. B. Raschke, C. Lienau, T. Hertel, H. Qian, A. J. Meixner, and A. Hartschuh, "Exponential decay lifetimes of excitons in individual single-walled carbon nanotubes," Phys. Rev. Lett. **95**(19), 197401 (2005).
29. A. J. Siitonen, D. A. Tsyboulski, S. M. Bachilo, and R. B. Weisman, "Surfactant-dependent exciton mobility in single-walled carbon nanotubes studied by single-molecule reactions," Nano Lett. **10**(5), 1595–1599 (2010).
30. C. Georgi, M. Böhmler, H. Qian, L. Novotny, and A. Hartschuh, "Probing exciton propagation and quenching in carbon nanotubes with near-field optical microscopy," Phys. Stat. Solidi B **246**(11-12), 2683–2688 (2009).
31. A. Bouhelier, R. Bachelot, G. Lerondel, S. Kostcheev, P. Royer, and G. P. Wiederrecht, "Surface plasmon characteristics of tunable photoluminescence in single gold nanorods," Phys. Rev. Lett. **95**(26), 267405 (2005).
32. L. G. Cançado, A. Jorio, A. Ismach, E. Joselevich, A. Hartschuh, and L. Novotny, "Mechanism of near-field Raman enhancement in one-dimensional systems," Phys. Rev. Lett. **103**(18), 186101 (2009).
33. L. Novotny, and B. Hecht, *Principles of Nano-Optics* (Cambridge, 2006).
34. L. Novotny, E. J. Sánchez, and X. S. Xie, "Near-field optical imaging using metal tips illuminated by higher-order Hermite–Gaussian beams," Ultramicroscopy **71**(1-4), 21–29 (1998).
35. M. R. Beversluis, L. Novotny, and S. J. Stranick, "Programmable vector point-spread function engineering," Opt. Express **14**(7), 2650–2656 (2006).

1. Introduction

Semiconducting single-walled carbon nanotubes (SWNTs) are photoluminescent quasi-one-dimensional nanostructures with large potential for photonic and optoelectronic applications [1]. Optical excitation of nanotubes creates excitons, strongly bound electron-hole pairs with exciton Bohr radii on the order of few nanometers. Photoluminescence (PL) in nanotubes results from exciton recombination with rather small radiative rates on the order of 1/10 ns^{-1} [2]. Efficient non-radiative decay channels on the timescale of several tens of picoseconds lead to small PL quantum yields for carbon nanotubes on substrates. External control of optical transition rates and the angular distribution of the emission would thus be useful for improving the performance of nanotube based nanoscale light sources, photodetectors, and photovoltaic devices [3,4].

Nanoscale metallic antenna structures couple free propagating electromagnetic radiation to a local receiver or transmitter by exploiting enhanced near-fields. This scheme can be used to locally enhance absorption and emission rates of energy quanta in single quantum structures such as organic molecules and semiconductor quantum dots [5–7]. Prominent examples utilizing antenna phenomena in the visible range are surface enhanced Raman scattering (SERS) and surface enhanced fluorescence (SEF) [8,9]. Antenna-enhanced near-field microscopy is realized by raster-scanning a metallic tip across the sample, so called tip-enhanced near-field optical microscopy (TENOM), providing both high spatial resolution and increased detection sensitivity. TENOM attracted increasing attention during the last years as an important tool to investigate optical properties of systems far beyond the diffraction limit [10–13]. Since the signal amplification results from both enhancement of the excitation and the radiative rate the respective contributions cannot be quantified directly.

Metal nanoobjects modify the emission characteristics of a dipole as has been shown in a number of studies [14–18]. Kühn et al. investigated the influence of a metal nanosphere on the

#128057 - $15.00 USD Received 5 May 2010; revised 24 Jun 2010; accepted 6 Jul 2010; published 21 Jul 2010

angular radiation pattern and also the fluorescence spectrum of a single fluorescent molecule [16]. Taminiau et al. used metallized nanorods to investigate the coupling between single emitters and nano-antennas showing that it is connected to a process of angular redirection [17]. The authors also demonstrated experimentally that the polarization state of single molecules fluorescence is dominated by the antenna regardless of the orientation of the molecular dipole [18].

In this letter we report on the first observation of the photoluminescence radiation pattern of semiconducting SWNTs in the absence and in the presence of an optical antenna. In the first step we show that PL in the one-dimensional nanotubes can be described by dipolar emission. We then positioned a sharp gold tip in nanometer distance and investigated the result of the antenna-nanotube near-field interaction. The observed radiation pattern demonstrates that the radiative rate enhancement is accompanied by an angular redirection of the PL and a change in polarization. By comparing radiation patterns with and without the influence of the antenna we can distinguish between radiation emitted via nanotube and antenna. We complement the experiments by simulations of the radiation patterns that support the considerations of the antenna and the nanotubes as point dipoles. Analyzing our data we show how it is possible to distinguish and quantify radiation and excitation rate enhancement.

2. Experimental

The experimental setup is based on an inverted microscope combined with an x,y-piezo position stage for raster scanning a microscope coverslide through the focus of a high numerical aperture (NA) objective. The optical response is collected by the same objective and focused on an avalanche photo diode (APD) after spectral filtering (F). Alternatively, a Bertrand lens is used to form an image of the back focal plane (BFP) on a cooled charge coupled device (CCD). In this configuration we have direct access to the intensity distribution of the radiation in the BFP, representing the radiation pattern [19]. A schematic of the setup is shown in Fig. 1(a).

Detailed investigations of nanotube PL radiation patterns have been carried out using a microscope setup equipped with an orange HeNe laser operating at an excitation wavelength of λ_{ex} = 594 nm and a microscope objective with NA = 1.3. Our near-field optical setup is based on the same microscope configuration using a red HeNe laser at λ_{ex} = 633 nm that is converted into a radially polarized laser mode and a microscope objective with NA = 1.49. The PL radiation patterns were found to be identical on both setups confirming the experimental approach and the reproducibility of our results. Antenna-enhanced measurements were performed by positioning a sharp gold tip with a tip diameter of about 20 nm into the laser focus. A tuning-fork shear force feed-back mechanism was used to set the tip-sample distance to about 4 nm to avoid metal-induced quenching effects [20,21].

#128057 - $15.00 USD Received 5 May 2010; revised 24 Jun 2010; accepted 6 Jul 2010; published 21 Jul 2010

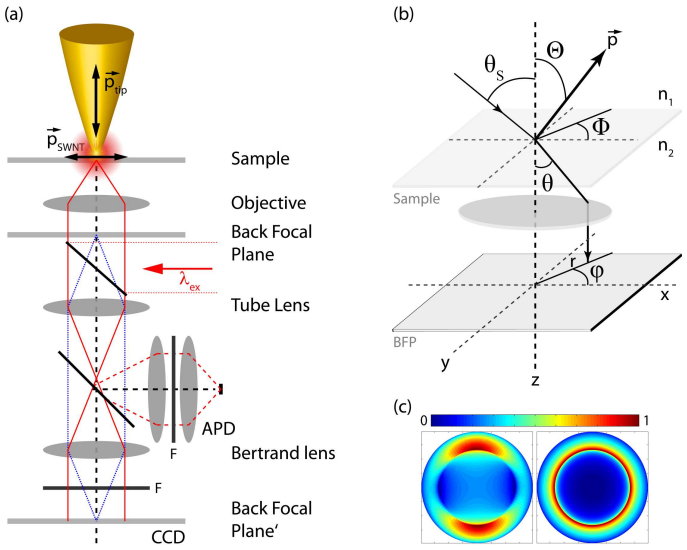

Fig. 1. Schematic of (a) the experimental setup and (b) the detection beam path including the parameters used in the simulations. Radiation patterns are recorded by imaging the back focal plane of the objective onto the CCD camera using the Bertrand lens. Simulated radiation patterns for point dipoles orientated horizontally (θ = 90°) and vertically (θ = 0°) are shown in (c) [24]. In (a) the orientation of SWNT dipole p_{SWNT} and metal tip dipole p_{tip} as determined experimentally are indicated.

We studied two types of sample material, sodium cholate wrapped CoMoCat SWNTs and SWNTs wrapped with poly(9,9-dioctyluorenyl-2,7-diyl) [22,23]. The nanotubes have a diameter in the range of one nanometer and are several hundreds of nanometers long. Radiation patterns detected after spin-coating on microscope coverslides were found to be identical for both materials.

Theoretical radiation patterns are calculated using the equations derived by Lieb et al. to describe a dipole close to a microscope coverslide and positioned in the focus of a high NA objective lens [24]. In this framework the intensity distribution I in the BFP of the objective is given by $I(r,\varphi,\Theta,\Phi) \sim \cos^{-1}(E_p E_p^* + E_s E_s^*)$ with the radial distance from the optical axis r, the azimuthal angle in the back aperture φ, the polar angle Θ and the azimuthal angle Φ of the dipole axis as depicted in Fig. 1(b). E_p and E_s are the p- and the s-polarized components of the electric field. Figure 1(c) shows calculated radiation patterns for a dipole oriented horizontally with respect to the substrate (left) and a vertically oriented dipole (right).

3. Radiation pattern of SWNTs

In the first step we acquired confocal PL images of SWNTs wrapped with sodium cholate that were spin coated on a glass coverslide. Luminescent SWNTs were localized by raster scanning the sample through the focus of a linearly polarized Gaussian laser beam and simultaneous detection of the nanotube PL signal in the range of the E_{11} transition between 880 and 1000 nm. Thereafter we center a single carbon nanotube with strong PL on the optical axis and record the angular emission pattern. Figure 2 shows an image scan (a) and three representative radiation patterns (b-d). In (e-f) theoretical dipolar emission patterns are shown for which the dipole orientation has been fitted to match the experimentally observed patterns in (b-d). The theoretical dipole patterns reproduce the radiation patterns from single nanotubes extremely well. Most intensity occurs in the outer ring which is the radiation emitted at an angle larger than the critical angle. The intensity is concentrated into two lobes on opposite sides of the patterns. Hence, the orientation of a dipole can be determined by fitting the simulated pattern to the measured data [24].

#128057 - $15.00 USD Received 5 May 2010; revised 24 Jun 2010; accepted 6 Jul 2010; published 21 Jul 2010

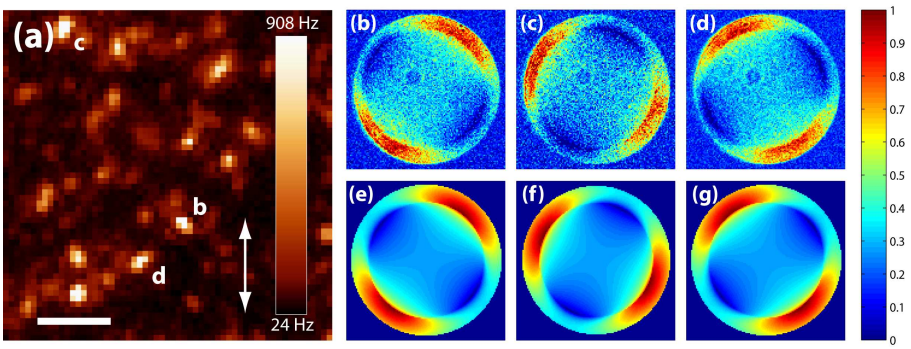

Fig. 2. (a) Confocal PL image of single SWNTs. The scale bar represents 2 µm. For three SWNTs marked in (a) the emission patterns are displayed (b-d) together with the corresponding simulated dipolar patterns (e-g). The angle Φ describing the in-plane dipole orientation has been varied to reproduce the corresponding experimental patterns.

All detected patterns can be modeled by in-plane dipoles with the polar angle Θ = 90°. This is in agreement with polarization resolved measurements and theoretical results from which nanotube PL from E_{11} transitions is known to be polarized along the nanotube axis and thus parallel to the sample surface [2]. In the examples in Fig. 2 the dipole axis and therefore the axis of the nanotubes were determined to be 142°, 61° and 35° with respect to the x-axis as defined in Fig. 1(b). Scanning a luminescent nanotube through the focus and recording an emission pattern at each pixel confirms that the intensity distribution does not depend on the position of the emitter relative to the focus. Only the signal to noise ratio changes and is best when the emitter is centered accurately in the focus (data not shown).

The excellent agreement between experimentally observed and simulated patterns indicates that exciton recombination in single carbon nanotubes of the present materials leads to dipolar emission. Exciton mobility described by center of mass motion will result in a random distribution of recombination sites along the nanotube axis [25,26]. Our results also show that PL emission does not couple to spatially extended antenna modes of the nanotube with narrow angular radiation patterns that are predicted in the case of elastic light scattering [27].

4. Radiation pattern in the presence of an optical antenna

The next step was to bring the near-field probe in the vicinity of an emitting SWNT. To confirm the correct position of the tip in the center of the focus and to prove that it provides high near-field enhancement we first recorded a PL image showing that the optical resolution is given by the near-field enhancement due to the tip, i.e. about 20 nm. For later comparison and analysis we then acquired a radiation pattern in the absence of the tip, denoted as PL^{0}_{SWNT}. Afterwards the gold tip was approached to acquire a second pattern PL^{*} with the nanotube underneath the tip. A representative data set is shown in Fig. 3. The near-field PL image (Fig. 3(a)) shows a bright SWNT with uniform intensity together with the simultaneously obtained topography as inset. Figure 3(c) shows the radiation pattern PL^{0}_{SWNT} detected without gold tip. Fitting this pattern results in a nanotube orientation of Θ = 148°. The orientation is confirmed by the topographical information obtained during the image scan.

In Fig. 3(b) the radiation pattern PL^{*} with the tip close to the nanotube is pictured. The pattern has changed considerably compared to the pattern without tip (Fig. 3(c)). For better comparison the pattern without tip is plotted again in (d) with the same intensity scaling as in (b). The first observation is that the overall intensity has increased, the integration of the patterns results in roughly five times more photon counts. The additional intensity results from the signal enhancement due to the near-field probe. Secondly, and even more clearly, the angular distribution of the intensity has changed. Instead of the two lobes the pattern is now

#128057 - $15.00 USD Received 5 May 2010; revised 24 Jun 2010; accepted 6 Jul 2010; published 21 Jul 2010

dominated by a sharp ring close to the critical angle. This ring shaped radiation pattern is characteristic for a vertically oriented dipole (see Fig. 1(c)).

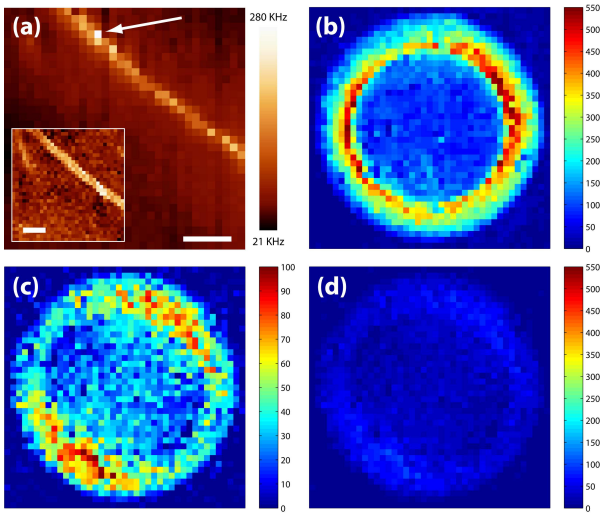

Fig. 3. (a) Near-field PL image of a SWNT with corresponding topography as inset. The scale bars represent 100 nm. (a-d) show emission patterns of the same SWNT in the vicinity of a gold tip (b) and without tip (c) and (d) measured at the position marked in (a). The intensity-scale in (d) is identical to that in (b) for better comparison.

Our data demonstrates that by bringing the tip close to the emitter a new channel for radiation is opened by which energy is transferred to the tip through near-field interaction. This energy is then emitted via the antenna dipole. In other words, the radiative rate of the nanotube and hence the ratio between emitted and absorbed photons is modified by adding the tip-induced radiative rate $k_{rad,tip}$. The radiative rate in the presence of the tip thus becomes $k^{*}_{rad} = k_{rad,SWNT} + k_{rad,tip}$ where $k_{rad,SWNT}$ is the radiative rate in the absence of the tip. The ring shaped pattern in Fig. 3(b) shows that emission via the tip antenna can be described by an axial point-dipole despite its semi-infinite structure.

In the following we analyze the observed signal enhancement and describe how excitation and radiative rate enhancement can be distinguished and quantified. This procedure exploits the different angular distributions of the emission via the in-plane nanotube dipole and the axially oriented tip dipole (see Fig. 1(c)). In the analysis we treat the nanotube and tip emitter independently leading to a superposition of the radiated intensities. Since the antenna emission is driven by the nanotube both emitters are coherent and we should in principle consider the interference of the radiated fields. However, since nanotube and tip dipoles are mutually perpendicular, the tip leads to radial polarization in the detected plane while the nanotube emission is linearly polarized. For most of the detected area the two fields are thus perpendicular. Moreover, in the area with parallel polarization, i.e. in the direction of the nanotube dipole, the intensity of the latter is very weak.

In general, the observed PL signal is the product of the detection efficiency of the system η, the PL quantum yield of the emitter Q and the excitation rate k_{ex}, giving $PL = \eta\gamma Q k_{ex}$. We have to take into account that the fraction γ of the total power radiated by a dipole into the angular detection range depends on the orientation of the dipole. In Fig. 4, γ is plotted vs. the maximum collection angle of the microscope objective θ_{max}. For our NA = 1.49 objective $\theta_{max} = 78.98°$ and the resulting fractions are $\gamma_{\parallel} = 0.73$ and $\gamma_{\perp} = 0.92$ for a horizontal and a vertical dipole, respectively. In the case of the antenna this quantity corresponds to the angular integral of the antenna directivity divided by 4π [17].

#128057 - $15.00 USD Received 5 May 2010; revised 24 Jun 2010; accepted 6 Jul 2010; published 21 Jul 2010

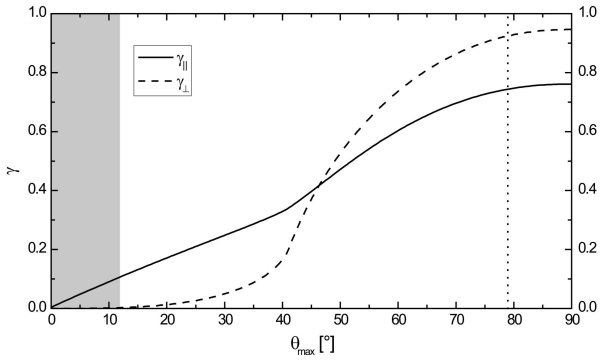

Fig. 4. Detected fraction γ of the total power radiated by a dipole oriented parallel (solid line) or perpendicular (dashed line) with respect to the substrate, depending on the collection angle of the microscope objective θ_{max}. The dotted line marks the maximum collection angle θ_{max} = 78.98° for the microscope objective with NA = 1.49. The gray area corresponds to the θ_{max} range for the inner part of the radiation patterns which was used to estimate F_{ex}. In this range the contribution of the vertical dipole is negligible.

The total signal detected by the CCD in the presence of the tip PL^* can be divided into two contributions, one that is radiated by the tip dipole PL^*_{tip} and the other that is radiated by the nanotube dipole PL^*_{SWNT}. The PL signal is given by

$$PL^*_{tip} = \eta\gamma_\perp Q^*_{tip}\frac{k^*_{ex}}{V} \tag{1}$$

for the tip dipole and

$$PL^*_{SWNT} = \eta\gamma_\parallel Q^*_{SWNT}\frac{k^*_{ex}}{V} + PL^0_{SWNT}\left(1-\frac{1}{V}\right) \tag{2}$$

for the nanotube dipole. PL^*_{SWNT} is the sum of the enhanced signal emitted by the nanotube dipole and the far-field background PL^0_{SWNT}. Q^*_{tip} and Q^*_{SWNT} are the quantum yields for the two emission channels given by the ratios $k_{rad,tip}/\sum k$ and $k_{rad,SWNT}/\sum k$ with the sum of all decay rates $\sum k = k_{rad,tip} + k_{rad,SWNT} + k_{nr}$ including the non-radiative rate k_{nr}. The factor V accounts for the different sizes of the confocal focus and the much smaller area underneath the tip in which the enhanced excitation and radiation takes place. In the example shown in Fig. 3 V is about 300 nm/20 nm = 15 as determined from the width of the PL signals in the confocal and near-field optical images (Fig. 2 and Fig. 3).

Let F_{ex} and F_{rad} denote the enhancement factors for the excitation rate and the radiative rate, respectively. The radiative rate enhancement factor F_{rad} is defined as $F_{rad} = k^*_{rad}/k_{rad} = 1 + k^*_{rad,tip}/k_{rad,SWNT}$. Using $Q^*_{tip}/Q^*_{SWNT} = k_{rad,tip}/k_{rad,SWNT}$ and Eqs. (1) and (2) we get F_{rad} by

$$F_{rad} = \frac{PL^*_{tip}\gamma_\parallel}{\left(PL^*_{SWNT} - PL^0_{SWNT}\left(1-1/V\right)\right)\gamma_\perp} + 1. \tag{3}$$

The intensity distribution of the emission radiated by the SWNT dipole in the absence of the tip PL^0_{SWNT} is known from the reference measurement (Fig. 3(c) and (d)). To proceed we need to separate the two contributions PL^*_{SWNT} and PL^*_{tip} to the signal observed with tip PL^*.

The radiation pattern from the axially oriented tip dipole shows nearly no intensity in the central part. The intensity ratio of the two patterns in the region θ_{max} = 0-12° (gray region in

#128057 - $15.00 USD Received 5 May 2010; revised 24 Jun 2010; accepted 6 Jul 2010; published 21 Jul 2010

Fig. 4) therefore reflects the enhanced emission via the nanotube dipole due to the enhanced excitation F_{ex} of the nanotube which is given by

$$F_{ex} = \frac{k_{ex}^{*}}{k_{ex}} \approx \frac{\left(PL_{SWNT}^{*} - PL_{SWNT}^{0}\right)V}{PL_{SWNT}^{0}} + 1. \quad (4)$$

In Eq. (4) we used the fact that exciton decay in nanotubes on substrates is dominated by non-radiative relaxation with $k_{nr} >> k_{rad,SWNT}$ leading to PL quantum yields on substrates below 0.01 [2,28]. Since we expect and also observe moderate radiative rate enhancement factors F_{rad} we can neglect the small reduction in quantum yield of PL emission via the nanotube dipole caused by the tip.

In the example shown in Fig. 3, F_{ex} is estimated to be 32 according to Eq. (4). This means that 32 times more excitons have been created in the presence of the antenna. According to Eq. (3) the radiative rate enhancement F_{rad} in our example was determined to be 1.9, showing that about 90% additional PL is radiated via the tip antenna.

The definition of $k_{rad,tip}$ is valid only for non-mobile excited states, such as in single fluorescent molecules and semiconductor nanocrystals, for which the distance between excited state and tip is fixed. Excitons in SWNTs however are highly mobile along the nanotube with a diffusion range of about 100 nm that was determined experimentally for SWNTs on substrates [25,26,29]. Therefore, a substantial fraction of excitons created by tip-enhanced excitation can leave the narrow near-field interaction range and thus the region of local radiative rate enhancement [30]. Radiative relaxation of these excitons then leads to in-plane dipolar emission contributing to the pattern denoted PL_{SWNT}^{*}. This means that the typical treatment for 0D structures underestimates the actual radiation enhancement factor F_{rad} in the case of higher-dimensional systems. We simulated the competition between exciton diffusion and local radiative rate enhancement by calculating the time-dependent spatial distribution of the exciton density after local antenna enhanced excitation using a 1D random-walk model [30]. Taking the diffusion range of 100 nm and the spatial extension of the near-field interaction of 20 nm as the only input parameters results in a significantly higher tip-mediated radiative rate $k_{rad,tip}$. The actual radiative rate enhancement factor F_{rad} in our example thus is 7.8.

Enhancement factors observed for different nanotubes and metal tips ranged from F_{ex} = 12-32 and F_{rad} = 6.1-13.6. The variation of enhancement factors is attributed to non-optimal positioning of the tip ontop of the nanotube and minor differences in tip shapes leading to a variability of antenna efficiencies.

For all investigated SWNTs and gold tips excitation enhancement was substantially more efficient than radiation enhancement even after accounting for exciton mobility. We can identify two reasons for this observation. First, there is a stronger field enhancement at the excitation as compared to the emission frequency. PL spectra of metal nanostructures are known to reflect the wavelength dependence of the field enhancement which is dominated by plasmon resonances in the visible range [31]. PL spectra of our tips (data not shown) peak in the range of the excitation wavelength at 633 nm used in the experiments, while the intensity at the emission wavelength of 950 nm is at least 20 times smaller.

The second reason for dominating excitation enhancement is based on the polarization of absorbing and emitting states. Emission at the exciton energy E_{11} is polarized in-plane as can be seen from the radiation patterns and the literature cited above. Treating the near-field interaction between tip and nanotube as dipole-dipole coupling only weak effects are expected due to the orthogonal orientation of the dipoles. In principal, radiative rate enhancement would be expected to occur twice along the nanotube at opposite sites displaced from the tip center [17]. On the other hand, excitation at 633 nm is within the range of the E_{12} transition of the investigated SWNTs that is polarized perpendicular to the nanotube axis [2]. For propagating fields this absorption is screened efficiently by the nanotubes' polarizability. However, since strongest field enhancement is obtained for these perpendicular fields more efficient excitation at E_{12} can be expected in the presence of the tip [32].

#128057 - $15.00 USD Received 5 May 2010; revised 24 Jun 2010; accepted 6 Jul 2010; published 21 Jul 2010

We note that a horizontally oriented dipole in the tip induced by the nanotube can also contribute to the radiation pattern detected as PL^{*}_{SWNT}. However, its contribution will be small compared to that of the vertical tip dipole due to the small polarizability of the tip perpendicular to its axis [33]. For a complete quantification of the respective contributions the one-dimensional structure of the nanotube needs to be considered. This could be done by spatially integrating the radiative rate modifications predicted for increasing in-plane tip sample-distance [17] corresponding to a coordinate along the nanotube axis. Since radiative rate enhancement is limited due to strong competition by exciton mobility as discussed before, the small contribution of the horizontal tip dipole can also be neglected compared to that of emission via the nanotube dipole. We estimate the uncertainty introduced by neglecting the horizontal tip dipole to be smaller than 10%.

In our experiments we observed deviations from perfect radial symmetry of the radiation pattern induced by the tip that can be attributed to non-ideal tip shapes. We remark that the radial polarization of the tip emission implicates that the tip antenna is excited efficiently using a radially polarized donut mode [34]. In general, the radiation pattern detected for a given antenna system will reflect the optimum excitation pattern at the detected frequency, as a consequence of reciprocity. After detecting the radiation pattern of a given antenna, its coupling efficiency could be optimized by vector point spread function engineering [35].

5. Summary

We showed that a photoluminescent SWNT on a dielectric substrate can be described by a single in-plane point dipole. The signal enhancement due to an optical antenna originates from enhanced excitation and additional radiation via the tip dipole along with spatial redirection of the emission. Analyzing the radiation patterns in the back focal plane of the microscope objective we estimated the enhancement factors of excitation F_{ex} and radiation F_{rad}. Our results illustrate that optical antennas could be used to improve the performance of carbon nanotube based nanoscale NIR emitters and absorbers.

Acknowledgments

We acknowledge Giovanni Piredda for helpful discussion. This work was funded by the Deutsche Forschungsgemeinschaft ((DFG-HA4405/3-1), ERA NanoSci (DFG-HA4405/5-1) and the Nanosystems Initiative Munich (NIM)), the National Science Foundation (DMR-0520513, EEC-0647560 and DMR-0706067) and the Nanoelectronics Research Initiative.

#128057 - $15.00 USD Received 5 May 2010; revised 24 Jun 2010; accepted 6 Jul 2010; published 21 Jul 2010